



# The influence of the $\alpha$ – $\beta$ phase transition of quartz on fluid inclusions during re-equilibration experiments



Gerald Doppler\*, Ronald J. Bakker

Department of Applied Geological Sciences and Geophysics, Chair of Resource Mineralogy, University of Leoben, Austria

## ARTICLE INFO

### Article history:

Received 19 December 2013

Accepted 16 March 2014

Available online 29 March 2014

### Keywords:

Fluid inclusion

$\alpha$ – $\beta$  quartz

Diffusion

Re-equilibration

Experimental study

H<sub>2</sub>O/D<sub>2</sub>O

## ABSTRACT

The influence of the  $\alpha$ – $\beta$  quartz phase transition on the properties of fluid inclusions was investigated experimentally. The experiments were designed to have no gradients in pressure and fugacity between fluid inclusions and pore fluid. Deformation due to pressure differences were also excluded in this study. H<sub>2</sub>O-rich fluid inclusions with similar densities were synthesized in quartz at approximately 625 °C and 280 MPa in the  $\alpha$ -quartz stability field, and at approximately 675 °C and 320 MPa in the  $\beta$ -quartz stability field. The experimental set-up prevented any pressure differences during loading and unloading of the experiments. These inclusions were re-equilibrated at the same temperature–pressure–fluid conditions, and changes in total homogenization temperature and ice melting temperature were recorded. Fluid inclusions are sensitive monitors of fluid conditions during entrapment, which record minor variation in temperature and pressure and display a corresponding distribution pattern in homogenization temperatures. Fluid inclusions re-equilibrated in the  $\alpha$ -quartz stability field were not affected by changes in density. Fluid inclusions re-equilibrated in the  $\beta$ -quartz stability field revealed density loss of –0.6% at 320 MPa to –3.0% at 280 MPa, which was caused by the  $\alpha$ – $\beta$  quartz phase transition. Consequently, density loss, which is probably caused by the formation of micro-cracks at the transition from  $\alpha$ - to  $\beta$ -quartz is more efficient at lower pressures. In addition, re-equilibration experiments were performed with a pure D<sub>2</sub>O pore fluid, to investigate diffusion processes at these experimental conditions. Diffusion of D<sub>2</sub>O is more efficient in  $\beta$ -quartz stability field, and may result in near total exchange of the original H<sub>2</sub>O content within only 19 days. Fluid inclusions re-equilibrated in the  $\alpha$ -quartz stability field contain only half the amount of D<sub>2</sub>O within the same experimentation run time, up to 53 mol% D<sub>2</sub>O.

© 2014 Elsevier B.V. All rights reserved.

## 1. Introduction

Phase changes of polymorphic minerals result in a variety of changes in physical and chemical properties, such as molar volume and heat capacities (e.g. Heuer and Nord, 1976), which may also affect hosted fluid inclusions. SiO<sub>2</sub> can crystallize in a variety of polymorphs at varying temperature and pressure, where  $\alpha$ -quartz is stable at relative shallow crustal conditions and  $\beta$ -quartz at higher temperatures in deep rock (e.g. Hosieni et al., 1985). Fluid inclusions in  $\alpha$ -quartz are important research objects (e.g. Samson et al., 2003), and their formational conditions can be interpreted from careful analysis of their fluid properties (composition and density) based on the closed-system assumption after trapping (e.g. Roedder, 1984). Some experimental work that addressed this assumption was performed within the  $\beta$ -quartz stability field (Sterner and Bodnar, 1989; Vityk and Bodnar, 1995, 1998), whereas changes of synthetic fluid inclusions within the  $\alpha$ -quartz field were investigated by Bakker and Diamond (1999), Bakker and Jansen (1990, 1991, 1993, 1994a, 1994b), and Doppler et al. (2013). Textural

information utilizing the distribution, morphology and surroundings of natural fluid inclusion is a major line of evidence for identifying the occurrence of post-entrapment changes in natural rock (e.g. Audétat and Günther, 1999; Ayllón et al., 2003). Diamond et al. (2010) and Tarantola et al. (2010) investigated experimentally changes in natural fluid inclusions that were imposed to deviatoric stress within the  $\alpha$ -quartz stability field close to the phase transition boundary.

The effect of the  $\alpha$ – $\beta$  quartz phase change on fluid inclusion properties during these experiments was not identified or systematically analyzed in these experimental studies and changes were only assigned to temperature and pressure of hydrothermal pore fluids. Consequently, these studies cannot identify definitely the individual processes that are independent of the  $\alpha$ – $\beta$  quartz transition, which may cause fluid inclusion alteration. Decrepitation experiments (e.g. Hladky and Wilkins, 1987) illustrated a relative intense acoustic emission at about the  $\alpha$ – $\beta$  quartz phase boundary at atmospheric pressures, interpreted to correspond to changes in the Young's modulus of quartz. The change in elasticity is most probably not accompanied with an acoustic effect during heating a quartz grain, because the effect is irreversible (pers. comm. B. Kingsley) and most likely to be related to the decrepitation of all smaller-sized fluid inclusions in a sample. Hall and Bodnar (1989)

\* Corresponding author.

E-mail address: [gerald.doppler@unileoben.ac.at](mailto:gerald.doppler@unileoben.ac.at) (G. Doppler).

carried out decrepitation experiments on heated natural fluid inclusion samples at room pressures in order to determine decrepitation profiles. They suggested that only small inclusions do not decrepitate until the quartz  $\alpha$ - $\beta$  transition temperature of 573 °C. Schmidt-Mumm (1991) identified the process of formation and propagation of micro-cracks as the origin of acoustic emission. Fluid inclusion decrepitation is only partly responsible for this emission, whereas the massive emission around the quartz  $\alpha$ - $\beta$  transition at 573 °C was suggested to result mainly from stress induced twinning according to the Dauphiné law (Laughner et al., 1979). Branlund and Hofmeister (2007) discovered a change of thermal diffusivity near 573 °C that is associated with the  $\alpha$ - $\beta$  quartz transition. The authors recognized exceeding thermal diffusivity of  $\beta$ -quartz that is most probably due to the expansion of the crystal lattice after crossing the phase boundary.

The present study is focused on the effect of the  $\alpha$ - $\beta$  quartz phase transition on the properties of H<sub>2</sub>O-rich synthetic fluid inclusions at higher pressures. Three types of experiments are performed: 1. Fluid inclusions are synthesized at specific conditions in the  $\alpha$ -quartz stability field close to the transition, and re-equilibrated at the same conditions (i.e. temperature, pressure and a H<sub>2</sub>O fluid). 2. A similar experiment is conducted within the  $\beta$ -quartz stability field, where it must be noted that loading and unloading of experiments must occur through the  $\alpha$ -quartz stability field. 3. Similar experiments within the  $\alpha$ -quartz and  $\beta$ -quartz stability field, with a D<sub>2</sub>O fluid instead of a H<sub>2</sub>O pore fluid during the re-equilibration experiments (see also Doppler et al., 2013) are performed to demonstrate diffusion. All synthesis and complementary re-equilibration experiments are carried out at the same temperature and pressure to have equal thermal activities and to exclude possible deformation. Re-equilibration experiments at the same conditions on either side of the  $\alpha$ - $\beta$  quartz phase transition will illustrate solely the effect of the phase transition on properties of fluid inclusions. Differences in chemical potential such as fugacity gradients between internal and external fluid represent an important parameter that affects bulk diffusion through a crystal (e.g. Bakker, 2009; Crank, 1975). In the case of higher pore fluid-fugacities relative to the fluid-inclusions in the host crystal, diffusion into the crystal is expected. Reverse fluid movement behavior would occur if internal fluid fugacity is higher compared to the pore fluid fugacity. As the ambient  $P$ - $T$  conditions are controlled by the computerized laboratory equipment and the composition of the loaded fluid species are well known, fluid fugacities can be easily calculated using the appropriate equations of state (e.g. Haar et al., 1984; Hill et al., 1982). By using pure D<sub>2</sub>O during re-equilibration

experiments, a gradient in chemical components is imposed, whereas the thermochemical properties are similar to H<sub>2</sub>O.

## 2. Experimental procedure and analytical methods

### 2.1. High $P$ - $T$ apparatus

Each experiment was synthesized and subsequently re-equilibrated in the hydrothermal laboratory at the University of Leoben. There are 10 Nimonic IOS/René 41 (Ni-Cr alloy) autoclaves installed, in a vertical position, as a cold-seal system similar to Kerrick (1987). Argon was used as the pressure medium ranging up to 1 GPa hydrothermal pressure. Temperature ranging up to 700 °C is induced by external furnaces. The sample temperature within the autoclaves is measured with an internal thermocouple directly monitoring and recording temperatures of the Au capsule, pre-loaded with the experimental material, consisting of partly cracked quartz rods and H<sub>2</sub>O or D<sub>2</sub>O. Temperature is controlled by a computerized operating system during the experiment and is measured with an uncertainty of 0.1 °C. Pressure is measured via pressure transducers, calibrated up to 700 MPa with a Heise dial gauge with an accuracy of 0.015%. Both temperature and pressure are continuously logged. The experimental setup stabilizes the synthesis conditions within 2 °C and 3 MPa during the experimental run-time of 19 days.

### 2.2. Fluid inclusion synthesis

Inclusion-free Brazilian quartz crystals were selected as starting material. Rods with a length of approximately 1 cm and a diameter of 2.75 mm are drilled along the quartz  $c$ -axis. The quartz rods are partially cracked by a thermal shock after heating to 400 °C. Arc-welded Au-capsules are used as containers during the experiments to prevent interaction with the autoclaves and the Ar-gas during the experiments. The capsules are loaded with the cracked quartz rod and approximately 0.07 g of ultra-pure H<sub>2</sub>O. The synthesis is performed by healing fractures according to the method of Bodnar and Sterner (1987). The experimental  $P$ - $T$  conditions of each experiment are given in Table 1 and Appendix A, and are illustrated in Figs. 1 and 2. All experiments are performed with a run-time of 19 days. The experiments are loaded and unloaded along specific isochores of the entrapped fluid to prevent stress that may cause deformation or cracking of inclusions due to internal fluid over- or under-pressure. Internal thermo-couples monitor the experimental  $P$ - $T$  conditions and provide the possibility to adjust conditions

**Table 1**

Experimental conditions and fluid properties of initial synthesis experiments (synth.) and corresponding re-equilibration experiments (re-eq.).

Experiment	$P^a$	$\pm P^b$	$T^c$	$\pm T^d$	$f^e$	$\pm f^f$	$V_m^g$	No. <sup>h</sup>
Blank H <sub>2</sub> O-H <sub>2</sub> O								
Synth. GMR009b	279.2	0.9	624.8	$\pm 0.7$	154.1	$\pm 0.8$	27.5	47
Re-eq. R009b	281.3	0.7	624.9	$\pm 0.3$	155.5	$\pm 0.5$	27.4	49
Synth. GMR010b	322.5	0.8	674.8	$\pm 0.6$	204.4	$\pm 0.9$	27.5	58
Re-eq. R010b	319.9	1.0	675.2	$\pm 0.3$	202.8	$\pm 0.8$	27.6	45
$\alpha$ -Quartz H <sub>2</sub> O-D <sub>2</sub> O								
Synth. GMR009a	279.2	0.9	624.8	$\pm 0.7$	154.1	$\pm 0.8$	27.5	68
Re-eq. R009a	278.7	2.3	624.9	$\pm 0.5$	154.0*	$\pm 1.4$	27.5*	63
$\beta$ -Quartz H <sub>2</sub> O-D <sub>2</sub> O								
Synth. GMR010a	322.5	0.8	674.8	$\pm 0.6$	204.4	$\pm 0.9$	27.5	100
Re-eq. R010a	321.1	1.1	674.8	$\pm 0.9$	203.8*	$\pm 1.2$	27.3*	94
Synth. GMR013a	280.3	1.1	674.7	$\pm 0.5$	175.6	$\pm 1.0$	29.2	60
Re-eq. R013a	279.4	0.9	674.7	$\pm 0.7$	175.2*	$\pm 0.9$	29.0*	60

<sup>a</sup> Pressure (MPa).

<sup>b</sup> Pressure variation (MPa).

<sup>c</sup> Temperature (°C).

<sup>d</sup> Temperature variation (°C).

<sup>e</sup> Fluid fugacity (in MPa) of H<sub>2</sub>O (Haar et al., 1984) and \*D<sub>2</sub>O (Hill et al., 1982) calculated with software from Bakker (2003; <http://fluids.unileoben.ac.at>).

<sup>f</sup> Fluid fugacity variation (MPa).

<sup>g</sup> Fluid molar volume (in cm<sup>3</sup>·mol<sup>-1</sup>) of H<sub>2</sub>O (Haar et al., 1984) and \*D<sub>2</sub>O (Hill et al., 1982) calculated with software from Bakker (2003; <http://fluids.unileoben.ac.at>).

<sup>h</sup> Number of measured fluid inclusions.

\* D<sub>2</sub>O fluid.

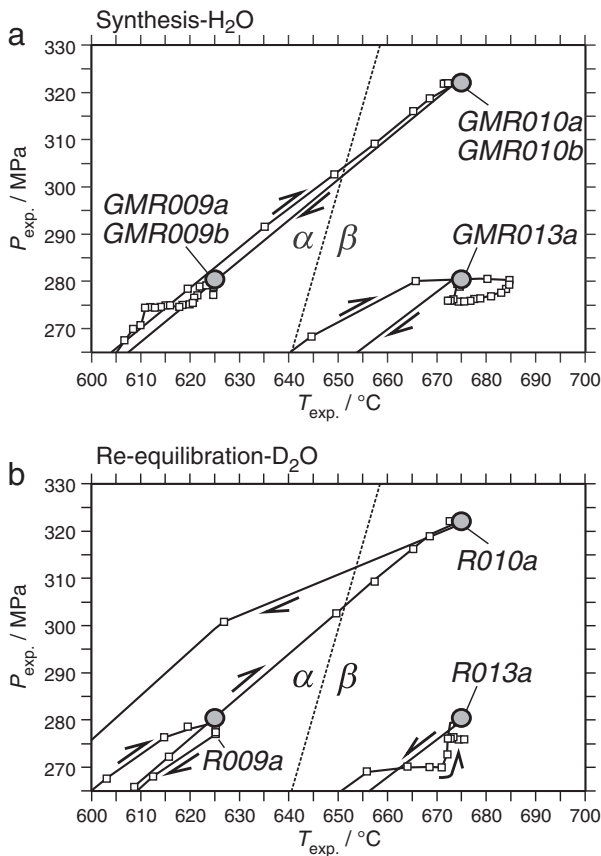


**Fig. 1.** Experimental  $P$ - $T$  conditions based on the computerized logging-system of the hydrothermal laboratory. The curves illustrate the loading (upward arrows) and unloading (downward arrows) of the sample conditions with a logging interval of 5 min (filled squares). (a) Conditions of the initial synthesis experiments with  $\text{H}_2\text{O}$  fluid and (b) conditions of the complementary re-equilibration experiments with  $\text{D}_2\text{O}$  fluid. The gray filled circles illustrate the average experimental conditions (see Table 1).

to obtain the desired fluid density. After the initial synthesis experiments the quartz rods are cut into disks and subsequently polished on both sides to a thickness of approximately 0.5 mm for subsequent microthermometric analyses and re-equilibration experiments.

### 2.3. Re-equilibration of fluid inclusions

After microscopic and microthermometric investigations the same quartz disks were used for re-equilibration experiments. Quartz disks were loaded in gold capsules supported by two quartz rods of the same diameter on both sides to prevent any damage of the relative fragile sample. Two re-equilibration experiments were performed with pure  $\text{H}_2\text{O}$  (experiments  $R009b$  and  $R010b$ ; Table 1 and Appendix A) and are designed to have similar conditions as the original synthesis experiment. Three re-equilibration experiments were performed by using pure  $\text{D}_2\text{O}$  as the quartz surrounding medium (experiment  $R009a$ ;  $R010a$ ;  $R013a$ ; see Table 1). Also here loading and unloading of the hydrothermal pressure vessels was performed according to specific isochore to minimize any pressure gradients between the synthesized fluid inclusions and the external fluid. The experimental  $P$ - $T$  conditions of each re-equilibration experiment are shown in Table 1 and illustrated in Figs. 1 and 2. Each re-equilibration experiment was carried out with a run-time of 19 days. The pressure and temperature conditions are stabilized within 2 °C and 3 MPa. After the re-equilibration experiments the same fluid inclusions from the initial synthesis were re-examined to compare inclusions density, composition and morphology and to detect changes in these parameters.

### 2.4. Microthermometry and optical analysis of shape, size and distribution within the quartz disk

Fluid inclusion properties of each individual fluid inclusion were characterized and analyzed as described in Doppler et al. (2013). Each assemblage (pre- and post-equilibration) was analyzed by cataloging various properties of up to 100 fluid inclusions, i.e. 1) each inclusion was photographed for documenting the morphological properties such as shape and size, and for identification purposes; 2) depth below the crystal surface; 3) the fluid inclusion composition and density is analyzed by microthermometry and Raman spectroscopy. A compilation of several acquired parameters of each individual inclusion is added in Appendix B. Changes in morphology are based on the shape definitions according to Bakker and Diamond (2006). The shape changes of individual fluid inclusions after re-equilibration are defined according to the relative change in inclusion perimeter/area ratio in two dimensional images, and the relative change in the major/minor axis ratio of the best-fit ellipse. The volumes of individual phases (liquid/vapor ratio) were difficult to obtain; therefore, area fractions of the vapor bubble ( $a_{\text{vap}}$ ) of each fluid inclusion were digitally measured from two-dimensional images by tracing the outside edge of the total inclusion and by the outside rim of the vapor bubble at room temperature. The distance of fluid inclusions to the crystal surface is measured with an optical microscope table that is adjustable in the  $z$ -direction (Olympus BX60). Both density and composition were obtained from homogenization and melting temperatures of the entrapped fluids, which were measured using a LINKAM MDS 600 and LINKAM THMSG 600 heating-freezing stages. The quality of the results of the Linkam MDS600 stage is determined by accuracy and precision of individual measurements. The instrument resolution of temperature measurements is 0.1 °C. The selection of thermodynamically determined temperatures of invariant points of phase changes measured in synthetic fluid inclusions with pure  $\text{H}_2\text{O}$  and a mixture of  $\text{H}_2\text{O}$  and  $\text{CO}_2$ , allows an excellent method to estimate the trueness of the stage. The precision of the stage is obtained from a series of repeated measurements of the same parameter, e.g. the critical homogenization temperature of  $\text{H}_2\text{O}$  in synthetic fluid inclusions. Measurements of this standard within a period of six months (25 measurements) reveal an average critical temperature of 378.6 °C (not corrected by calibration), with a standard deviation of the sample of  $\pm 0.4$  °C, whereas the standard error in mean is  $\pm 0.1$  °C. The average melting temperatures of  $\text{H}_2\text{O}$  and  $\text{CO}_2$  are  $+0.4$  °C and  $-56.6$  °C (not corrected by calibration), respectively, with standard deviations of sample of  $\pm 0.1$  and  $\pm 0.2$  °C, respectively, and standard error in mean of  $\pm 0.0$  and  $\pm 0.1$  °C, respectively. It must be noted that the precision of the measurement of one inclusion can only be obtained by multiple measurements of the same object. It is assumed that the precision obtained from measurements of the standards is valid for measurements of individual fluid inclusions at similar temperatures. Knowledge of the exact temperatures of these invariant points, i.e. critical temperature of  $\text{H}_2\text{O}$  (374.0 °C), melting temperature of  $\text{H}_2\text{O}$  (0.0 °C) and  $\text{CO}_2$  ( $-56.6$  °C) is used for calibration, which is greatly improving the accuracy of individual measurements within the range of  $-56.6$  to  $+374.0$  °C. The  $\text{D}_2\text{O}$  composition was determined from the melting temperatures of the  $\text{D}_2\text{O}$ - $\text{H}_2\text{O}$  mixtures (see Doppler et al., 2013), as defined by significant differences in melting temperatures  $T_m(\text{SV} \rightarrow \text{LV})$  of pure  $\text{H}_2\text{O}$  (0.0 °C) and pure  $\text{D}_2\text{O}$  ( $+3.8$  °C). Relative amounts of  $\text{H}_2\text{O}$  and  $\text{D}_2\text{O}$  are obtained from Eq. (1)

$$x_{\text{rel}}(\text{D}_2\text{O}) = \frac{T_m(f_i)}{T_m^0(\text{D}_2\text{O}) - T_m^0(\text{H}_2\text{O})} \quad (1)$$

where  $T_m$  is the melting temperature in °C,  $f_i$  is the solution in a specific fluid inclusion. The superscript 0 indicates the pure phase. The presence of  $\text{D}_2\text{O}$  was also confirmed by Raman spectroscopy.

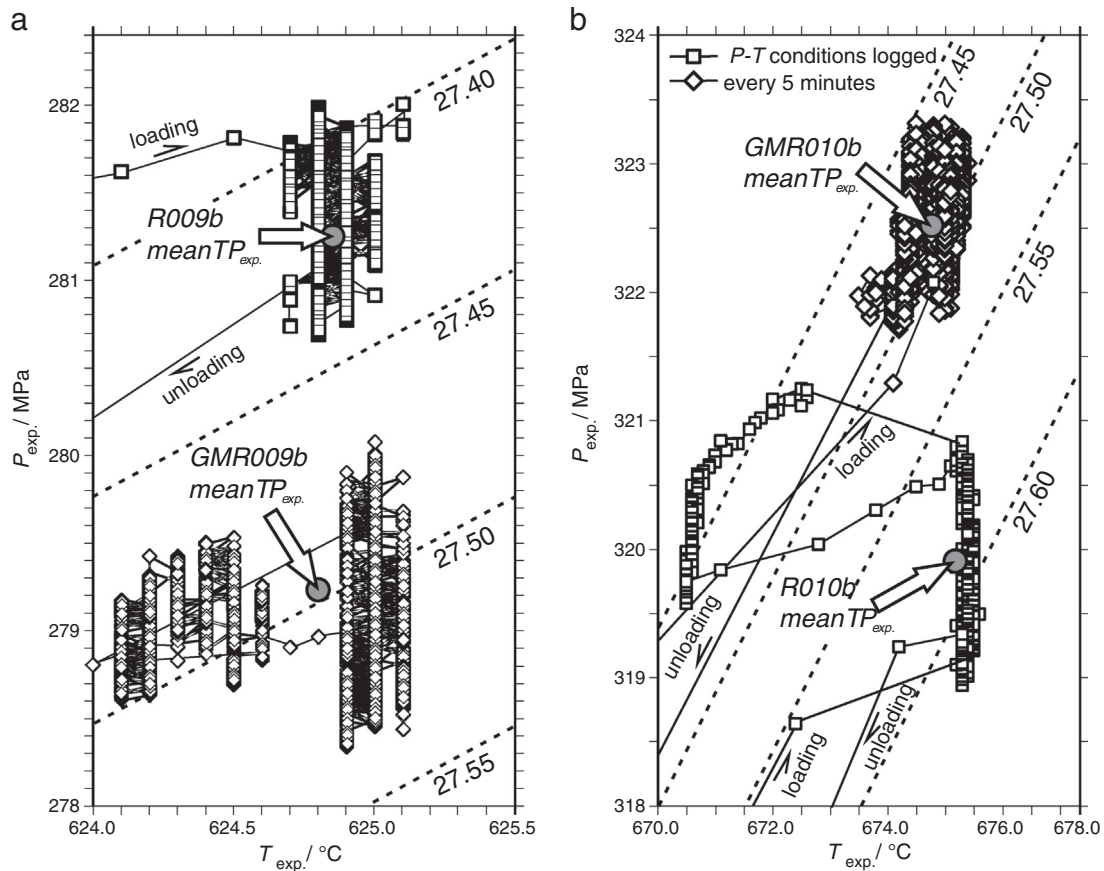


**Fig. 2.** Experimental pressure–temperature record of the blank experiments. The inclined dashed lines are isochores of pure  $H_2O$  (numbers in  $cm^3 \cdot mol^{-1}$ ). (a) The experimental  $P_{mean}$  of synthesis  $GMR009b$  is 279.2 MPa at the  $T_{mean}$  of 624.8  $^{\circ}$ C (gray filled circle) within the  $\alpha$ -quartz stability field. The experimental mean-conditions of the complementary re-equilibration  $R009b$  are 281.3 MPa and 624.9  $^{\circ}$ C. (b) The mean pressure of synthesis experiment  $GMR010b$  is 322.5 MPa at  $T_{mean}$  of 674.8  $^{\circ}$ C within the  $\beta$ -quartz stability field. The complementary re-equilibration conditions of  $R010b$  are  $P_{mean}$  of 319.9 MPa and 675.2  $^{\circ}$ C.

### 3. $H_2O$ – $D_2O$ fugacity, molar volume and calculated homogenization conditions

The fugacity and molar volume of pure  $H_2O$  and  $D_2O$  fluids were calculated with the equations of state of Haar et al. (1984) and Hill et al. (1982), respectively. These equations of state are included in the software package “FLUIDS” (Bakker, 2003; and <http://fluids.unileoben.ac.at>) in the programs “Loner HGK” and “Loner HCL”. The equation of

state for  $D_2O$  is limited to maximum values of 100 MPa and 600  $^{\circ}$ C, but was extrapolated to the experimental conditions in this study.

Four experiments have been performed along the  $H_2O$ -isochore of 27.5  $cm^3 \cdot mol^{-1}$  (Table 1): two within the  $\alpha$ -quartz stability field close to the transition conditions to  $\beta$ -quartz ( $GMR009a$  and  $GMR009b$ , Figs. 1 and 2), and two within the  $\beta$ -quartz stability field, just across the phase transition ( $GMR010a$  and  $GMR010b$ , Figs. 1 and 2). The calculated  $H_2O$  fugacities of these experiments are 154.1 MPa in the  $\alpha$ -quartz

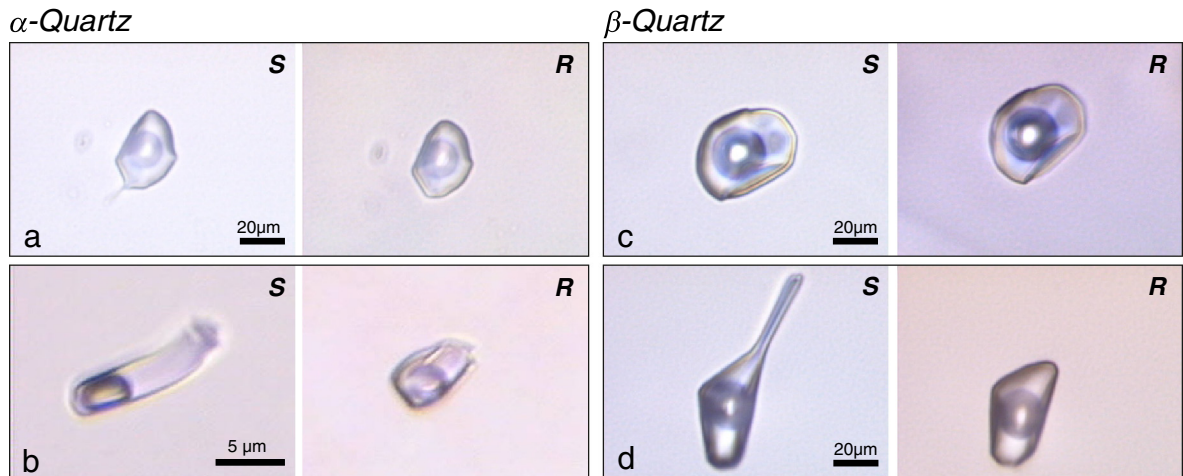


**Fig. 3.** Photomicrographs of the same inclusion before ( $S$  = synthesized) and after the blank re-equilibration experiments ( $R$  = re-equilibrated). Fluid inclusions of the experiments  $GMR009b$  and  $R009b$  are performed within the  $\alpha$ -field (a and b); and fluid inclusion examples of  $GMR010b$  and  $R010b$  are carried out within the  $\beta$ -quartz stability field (c and d).

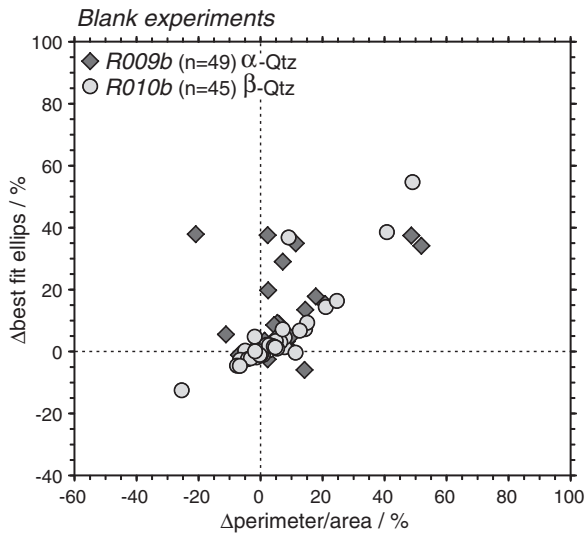


**Fig. 4.** Fluid inclusion shape diagram illustrating the magnitudes of shape changes during re-equilibration of the blank experiments. Terms are according to Bakker and Diamond (2006), see text for further details.

stability field and 204.4 MPa in the  $\beta$ -quartz stability field (Table 1). In addition, one experiment in the  $\beta$ -quartz stability field was performed at similar temperatures as the previously mentioned experiments, but modified pressures, resulting in molar volume of  $29.2 \text{ cm}^3 \cdot \text{mol}^{-1}$  (GMR013a, Fig. 1) with a corresponding  $\text{H}_2\text{O}$  fugacity of 175.6 MPa.

Homogenization conditions of the entrapped fluid in synthetic fluid inclusions were calculated by descending along the isochore from experimental conditions to the liquid–vapor curve, including isochore correction due to the thermal expansion and compressibility of the quartz host (Hosieni et al., 1985; and its rectification according to Sterner and Bodnar, 1991). The corrected isochores were calculated with the software “ISOC” (Bakker, 2003). Fluid inclusions from the initial synthesis experiments GMR009a and GMR009b should theoretically homogenize at  $320.5 \pm 0.6 \text{ }^\circ\text{C}$  and have a molar volume of  $27.05 \pm 0.40 \text{ cm}^3 \cdot \text{mol}^{-1}$  at this temperature. Uncorrected isochores result in homogenization temperatures of  $324.8 \pm 0.6 \text{ }^\circ\text{C}$ . Although the molar volume of the fluid in the experiments GMR010a and GMR010b is similar to GMR009a and GMR009b, the theoretical homogenization temperature along the host mineral corrected isochore is  $317.5 \pm 0.5 \text{ }^\circ\text{C}$ , whereas the uncorrected isochore also results in  $T_h = 324.8 \pm 0.5 \text{ }^\circ\text{C}$ . The corrected molar volume at homogenization conditions is  $26.75 \pm 0.40 \text{ cm}^3 \cdot \text{mol}^{-1}$ . Theoretical homogenization conditions of experiment GMR013a according to

corrected isochore is  $T_h = 332.3 \pm 0.5 \text{ }^\circ\text{C}$  (corresponding to  $28.40 \text{ cm}^3 \cdot \text{mol}^{-1}$ ). Uncorrected isochores result in  $T_h$  of  $337.9 \pm 0.5 \text{ }^\circ\text{C}$ .

Re-equilibration experiments with  $\text{H}_2\text{O}$  (R009b and R010b) are performed at the nearly the same conditions (Fig. 2) as the original synthesis experiments (GMR009b and GMR010b), and result in similar molar volumes, fugacities and theoretical homogenization temperatures. Re-equilibration experiments with  $\text{D}_2\text{O}$  at similar temperature and pressure in the  $\alpha$ -quartz stability field (R009a) and the  $\beta$ -quartz stability field (R010a and R013a) do not show significant different values in molar volume, fugacities and  $T_h$  from the original experiment.

## 4. Experimental results

### 4.1. $\text{H}_2\text{O}$ blank experiments

Most fluid inclusions synthesized in experiment GMR009b ( $\alpha$ -quartz) displayed minor changes in morphology after re-equilibration (experiment R009b; Figs. 3a, b and 4). The fluid inclusions are both equant and regular shaped or elongated and regular shaped. Initially the elongated fluid inclusions tend to become more equant after re-equilibration, and exhibit the highest magnitude in shape changes in Fig. 4. The inclusions that were originally equant and regular did not show shape change during re-equilibration. Morphological changes in the experiments GMR010b and R010b in the  $\beta$ -quartz stability field are similar to those changes in the  $\alpha$ -quartz field (Figs. 3c, d and 4). However, the change in shape parameters in the  $\beta$ -quartz experiment exhibit slightly higher values than the  $\alpha$ -quartz experiments (up to 60%).

Homogenization temperatures of the  $\text{H}_2\text{O}$  synthesis within the  $\alpha$ -quartz stability field of experiment GMR009b reveal a mean  $T_h$  of  $323.7 \text{ }^\circ\text{C}$ , a  $T_h$  mode between  $323.0$  and  $323.5 \text{ }^\circ\text{C}$ , and a variation from  $321.9$  to  $325.5 \text{ }^\circ\text{C}$  (Table 2 and Fig. 5a). Fig. 5a illustrates an irregular distribution of homogenization temperatures, i.e. the mode is at lower temperatures than the temperature obtained from a best-fit Gaussian distribution function. Changes in density (and molar volume) were observed even for the blank experiments simply by measuring the homogenization temperature of the fluid inclusions. During  $\alpha$ -quartz re-equilibration experiment R009b fluid inclusions altered to higher densities with a maximum shift in  $T_h$  up to  $-0.9 \text{ }^\circ\text{C}$  (see Fig. 6). Fluid inclusions with originally relatively low  $T_h$  have similar change in density as fluid inclusions with initially higher  $T_h$ . Experiment GMR010b was carried out within the  $\beta$ -quartz stability field and revealed a mean  $T_h$  of  $322.0 \text{ }^\circ\text{C}$  with a variability of  $\pm 2.6 \text{ }^\circ\text{C}$ . The mode of the  $T_h$  distribution is between  $322.0$  and  $323.0 \text{ }^\circ\text{C}$  (Table 2 and Fig. 5b). The  $T_h$  distribution of this experiment reveals a normal distribution (Gaussian). The change in  $T_h$  is opposite to the  $\alpha$ -quartz experiment, and reaches values up to

**Table 2**  
Homogenization temperatures of fluid inclusions from initial experiments and re-equilibration experiments, melting temperatures with corresponding  $\text{D}_2\text{O}$  content after re-equilibration.

Synth.	$T_h^a$	Max <sup>b</sup>	Min <sup>c</sup>	Re-equ.	$T_h^d$	Max <sup>e</sup>	Min <sup>f</sup>	Max. $T_m^g$	% $\text{D}_2\text{O}^h$
Blank $\text{H}_2\text{O}$ – $\text{H}_2\text{O}$									
GMR009b	323.7	+1.8	–1.8	R009b	323.2	+2.0	–1.7	0.0	–
GMR010b	322.0	+2.6	–2.6	R010b	323.2	+1.7	–1.5	0.0	–
$\alpha$ -Quartz $\text{H}_2\text{O}$ – $\text{D}_2\text{O}$									
GMR009a	323.7	+2.3	–2.4	R009a	322.3	+3.1	–1.9	2.6	68
$\beta$ -Quartz $\text{H}_2\text{O}$ – $\text{D}_2\text{O}$									
GMR010a	322.9	+3.9	–2.0	R010a	321.1	+2.4	–4.4	3.7	97
GMR013a	337.3	+1.6	–1.5	R013a	335.2	+2.7	–2.3	3.6	95

<sup>a</sup> Mean  $T_h$  (homogenization temperature) initial synthesis ( $^\circ\text{C}$ ).

<sup>b</sup> Maximum  $T_h$  – mean  $T_h$  initial synthesis ( $^\circ\text{C}$ ).

<sup>c</sup> Mean  $T_h$  – minimum  $T_h$  initial synthesis ( $^\circ\text{C}$ ).

<sup>d</sup> Mean  $T_h$  re-equilibration ( $^\circ\text{C}$ ).

<sup>e</sup> Maximum  $T_h$  – mean  $T_h$  re-equilibration ( $^\circ\text{C}$ ).

<sup>f</sup> Mean  $T_h$  – minimum  $T_h$  re-equilibration ( $^\circ\text{C}$ ).

<sup>g</sup> Maximum  $T_m$  (melting temperature) re-equilibration ( $^\circ\text{C}$ ).

<sup>h</sup> Maximum mole%  $\text{D}_2\text{O}$ .

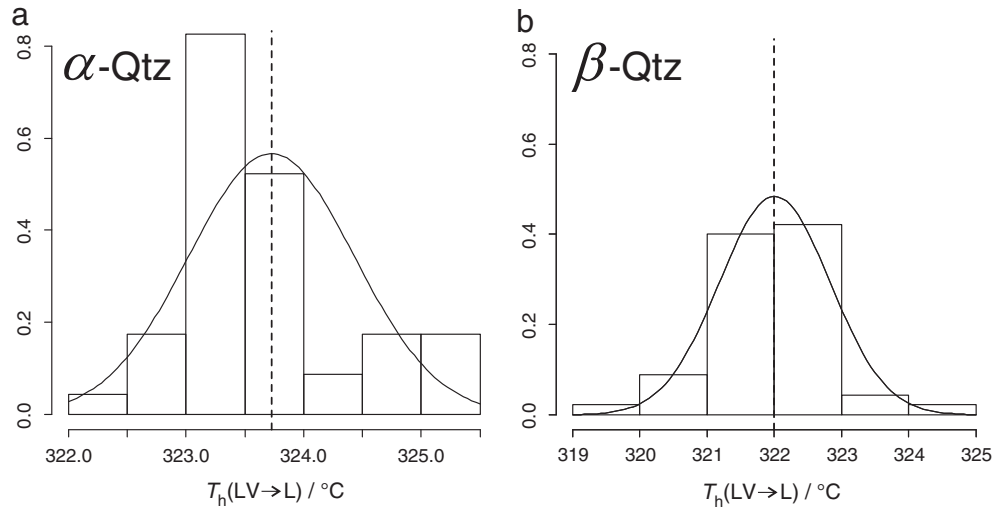


**Fig. 5.** Homogenization temperature histograms. (a) The  $\alpha$ -quartz experiment (GMR009b) gives the range of  $T_h$  from 321.9 to 325.5 °C with a median of 323.7 °C (dashed line) and a mode of 323.0 to 323.5 °C. (b) The histogram based on the data of the  $\beta$ -quartz experiment GMR010b gives the  $T_h$  range from 319.4 to 324.6 °C with a median of 322.0 °C (dashed line) and a mode of 322.0 to 323.0 °C. Both synthesis experiments show a normal distribution of the  $T_h$  values. Detailed fluid inclusion properties are summarized in Table 2 and in Appendix B.

+2.5 °C for inclusions with originally higher densities, whereas inclusions with initially lower densities only change about +0.3 °C (Fig. 6).

#### 4.2. D<sub>2</sub>O re-equilibration experiment in the $\alpha$ -quartz stability field

The majority of the synthesized fluid inclusions in the experiment GMR009a ( $\alpha$ -quartz) display no appreciable change in the inclusions shape during re-equilibration (experiment R009a; see Figs. 7a and 8a). The synthesized fluid inclusions are both equant and regular or elongated and irregular. Initially elongated and irregular inclusions tended to become more equant and regular during re-equilibration. These inclusions show the highest magnitude (up to 80%) in shape changes for these experiments (Figs. 7 and 8).

Homogenization temperatures of the synthesized H<sub>2</sub>O inclusions of the  $\alpha$ -quartz experiment GMR009a reveal a mean  $T_h$  of 323.7 °C with a variation of 321.3 to 326.0 °C (see Table 2). Density changes (and molar volume changes) were measured using the changes in the

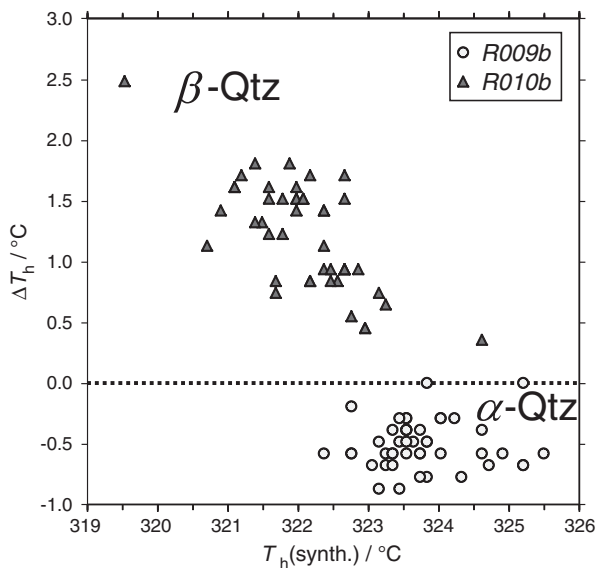


**Fig. 6.** Homogenization temperature of the initial synthesis (experiment GMR009b and GMR010b) versus the change in  $T_h$  of the complementary re-equilibration experiments R009b and R010b.  $\alpha$  illustrates the experiment in the  $\alpha$ -quartz stability field, and  $\beta$  in the  $\beta$ -quartz stability field.

homogenization temperatures of the re-equilibrated fluid inclusions. During  $\alpha$ -quartz re-equilibration experiment R009a, fluid inclusions altered to higher densities with a maximum shift in  $T_h$  up to  $-2.4$  °C (Fig. 9a). Changes in fluid inclusion composition after re-equilibration with D<sub>2</sub>O are calculated from the positive melting temperatures via Eq. (1) and are illustrated in Fig. 9. Experiment R009a reveals a maximum  $T_m(\text{ice})$  of +2.6 °C which corresponds to 68 mol% D<sub>2</sub>O (Fig. 9a). The long dashed line in Fig. 9a represents the expected changes in  $T_h$  with increasing D<sub>2</sub>O content as illustrated by increased  $T_m(\text{ice})$ . Re-equilibrated fluid inclusions in experiment R009a show a distribution of  $T_m$  and  $T_h$  which correspond to the expected composition.

#### 4.3. D<sub>2</sub>O re-equilibration experiment in the $\beta$ -quartz stability field

Fluid inclusions which were synthesized in the  $\beta$ -quartz stability field (experiment GMR010a and GMR013a) display similar changes in morphology after re-equilibration (experiment R010b and R013b; Figs. 8b and 10). Originally equant and regular inclusions display limited shape changes compared to fluid inclusions which are originally

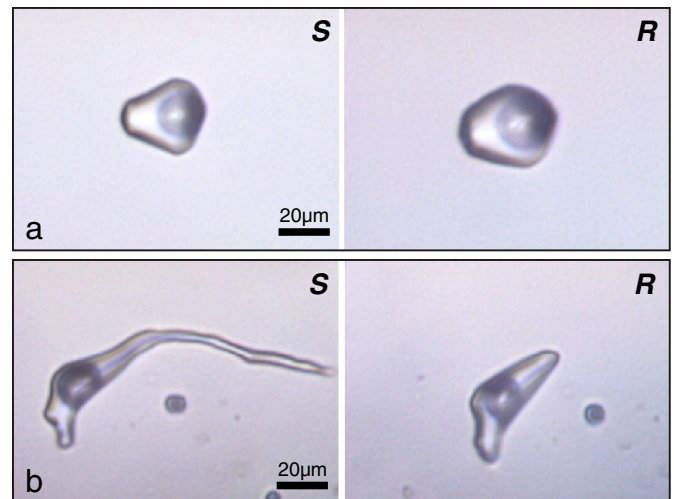


**Fig. 7.** Photomicrography of the same inclusions before (S = synthesized, GMR009a) and after re-equilibration experiments in D<sub>2</sub>O (R = re-equilibrated, R009a) which are performed in the  $\alpha$ -quartz field. Fluid inclusion with minor shape changes is illustrated in (a) and major shape changes in (b).

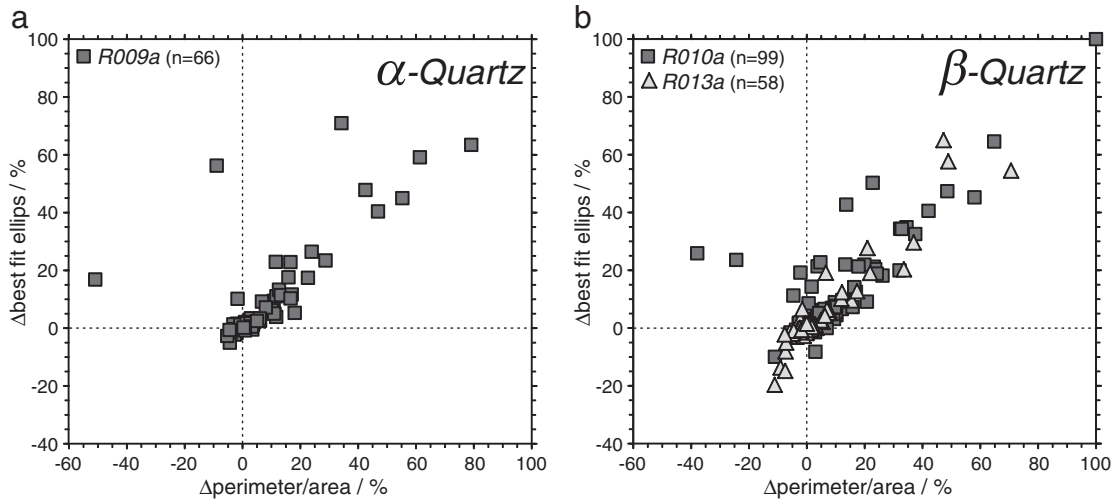


**Fig. 8.** Fluid inclusion shape diagram illustrating the magnitudes of shape changes of the re-equilibration experiment in the  $\alpha$ -quartz stability field with  $D_2O$  in (a) and in the  $\beta$ -quartz stability field with  $D_2O$  in (b). Terms are according to Bakker and Diamond (2006), see text for further details.

elongated and irregular. The distribution of the magnitude in shape changes during re-equilibration illustrates comparable values considering the stability field of quartz ( $\alpha$  versus  $\beta$ -quartz; Fig. 8a and b).

The synthesized  $H_2O$  inclusions of the experiment GMR010a display a mean  $T_h$  of 322.9 °C with a variation of 320.9 to 326.8 °C (Table 2). Homogenization temperatures of the fluid inclusions in experiment GMR013a display a mean  $T_h$  of 337.3 °C with a variation between 335.8 and 338.9 °C (Table 2). After re-equilibration in the  $\beta$ -quartz stability field density (and molar volume) changes were determined by measuring lower homogenization temperatures compared to the initial experiments. Both, experiment R010a and experiment R013a illustrate density increase (Fig. 9b), corresponding to a maximum shift in  $T_h$  of up to  $-3.0$  °C and  $-3.4$  °C, respectively. After re-equilibration with pure  $D_2O$ , the maximum ice melting temperature of experiment R010a is  $+3.7$  °C which corresponds to a fluid inclusion composition of about 97 mol%  $D_2O$ . The maximum  $T_m(\text{ice})$  value of the  $\beta$ -quartz experiment R013a is comparable to R010a with  $T_m$  values up to  $+3.6$  °C.

The long dashed lines in Fig. 9 illustrate the expected combination of homogenization temperature and melting temperature. The calculated

$T_h$  for inclusions that completely exchanged their  $H_2O$  content for  $D_2O$  in experiment R010a is 319.2 °C which corresponds to a  $\Delta T_h$  of  $-5.6$  °C (calculated with software package “FLUIDS”; Bakker, 2003). For the experiment R013a a maximum shift in  $T_h$  after total re-equilibration with  $D_2O$  is expected with a  $\Delta T_h$  of  $-7.0$  °C derived by a calculated  $T_h$  of 338.1 °C. The measurements from R009a in the  $\alpha$ -quartz stability field are approximately according to the expected trend in combinations of  $T_h$  and  $T_m$ , whereas R010a and R013a in the  $\beta$ -quartz stability field illustrate notably higher values of  $T_h$  than expected at selected  $T_m$  values.

## 5. Discussion

### 5.1. Morphological changes of fluid inclusions

According to the original assumptions only minor morphological changes of fluid inclusions can be observed after the presented re-equilibration experiments. Morphological changes are almost identical in  $\alpha$ -quartz and  $\beta$ -quartz. The morphological change rate is independent

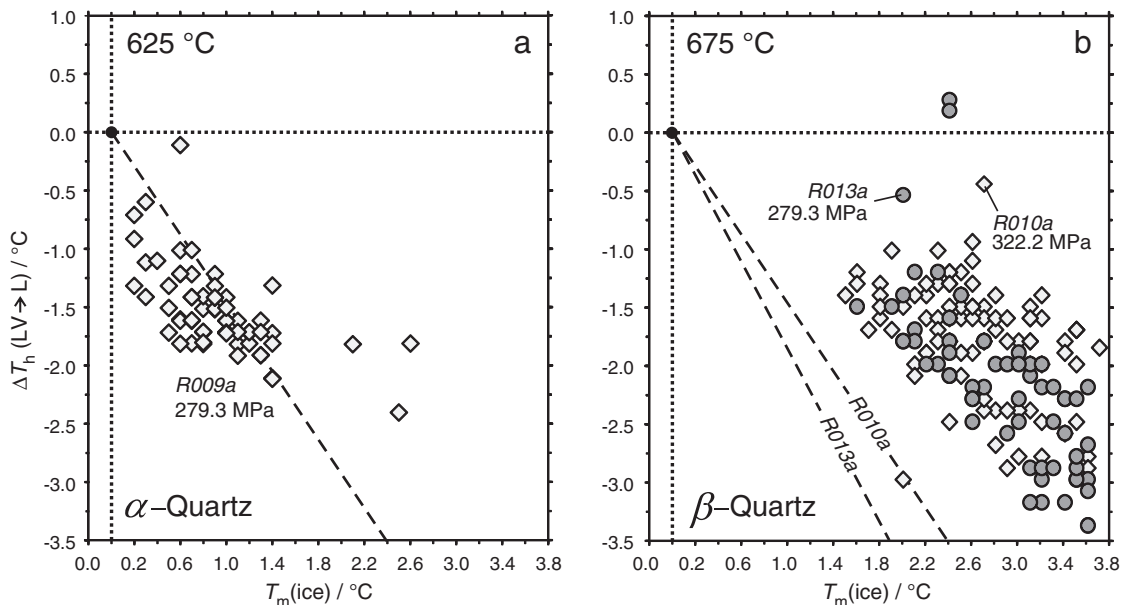


**Fig. 9.** Melting temperature of ice versus changes in homogenization temperature after the re-equilibration experiments R009a (a), R010a (b), and R013a (b) with  $D_2O$ .

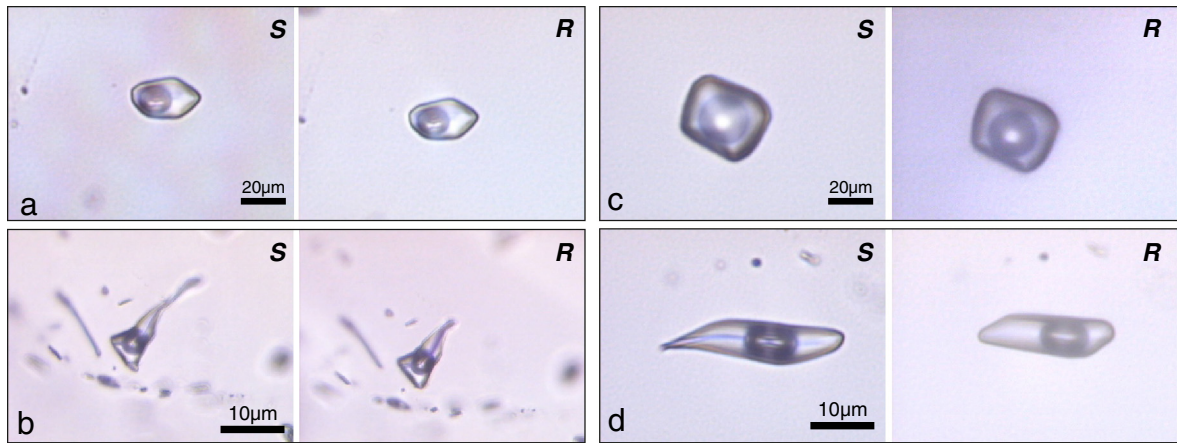


**Fig. 10.** Photomicrographs of the same inclusion before (*S* = synthesized) and after the re-equilibration experiments (*R* = re-equilibrated) with  $D_2O$ . Fluid inclusions of the experiments *GMR010a*, *R010a* (a and b) and *GMR013a* and *R013a* (c and d) are performed within the  $\beta$ -field.

of the quartz modification. Fluid inclusions tend to reach negative crystal shape during elevated hydrothermal  $P$ – $T$  conditions without respect to the quartz modification and without stress components. Irregular and elongated fluid inclusions show the highest shape change during re-equilibration. Morphological changes are independent of the pore fluid ratios  $H_2O/D_2O$ . The magnitude of fluid inclusions shape change is mainly temperature dependent and consistent with the results of Doppler et al. (2013).

### 5.2. Distribution pattern of $T_h$ in $H_2O$ blank experiments

The measured homogenization temperatures of the  $\alpha$ -quartz experiment *GMR009b* reveal an irregular distribution as illustrated in Fig. 5a. The corresponding histogram of the logged experimental pressure conditions (Fig. 11a) shows a similar irregular distribution, which deviates from a normal (Gaussian) distribution pattern. Therefore, the measured  $T_h$  of a fluid inclusion assemblage clearly reflects fluctuations in experimental  $P$ – $T$  conditions, and the fluid inclusion assemblage sensitively stores the ambient formation conditions. This can also be deduced from the second  $H_2O$  blank experiment *GMR010b* performed in the  $\beta$ -quartz field (c.f. Figs. 5b and 11b); both, the experimental conditions record of pressure and the measured  $T_h$  are normally distributed (Gaussian distribution). This phenomenon also illustrates that fluid

inclusions are continuously synthesized during the entire experimental run-time and not at a specific moment of experimentation. In natural rock, the distribution pattern of  $T_h$  in a fluid inclusion assemblage that did not re-equilibrate or change its properties after trapping must correspond to a variation in trapping conditions, probably caused by slightly varying pore fluid pressure.

### 5.3. Shift in $T_h$ in $H_2O$ blank experiments

According to the experimental variation in experiment *GMR009b* in the  $\alpha$ -quartz stability field (Fig. 2a), the molar volume of the entrapped fluid may vary between 27.47 and 27.54  $cm^3 \cdot mol^{-1}$ . The measured  $T_h$  (Fig. 5a), which directly reflect molar volumes, are slightly lower than the calculated  $T_h$  of “uncorrected” isochores (see paragraph 3), but significantly higher than  $T_h$  of “corrected” isochores. Consequently, isochore correction according to the compressibility and expansion of quartz result in overestimated density calculations. The complementary re-equilibration experiment *R009b* was performed at approximately 2 MPa higher pressures, with a variation in molar volume of 27.39 to 27.44  $cm^3 \cdot mol^{-1}$ . These slightly lower molar volumes result in minor modifications of  $T_h$ , i.e. a change of  $-0.2$  to  $-1.3$  °C. The observed changes in  $T_h$  (Fig. 6) agree with these theoretical predictions.

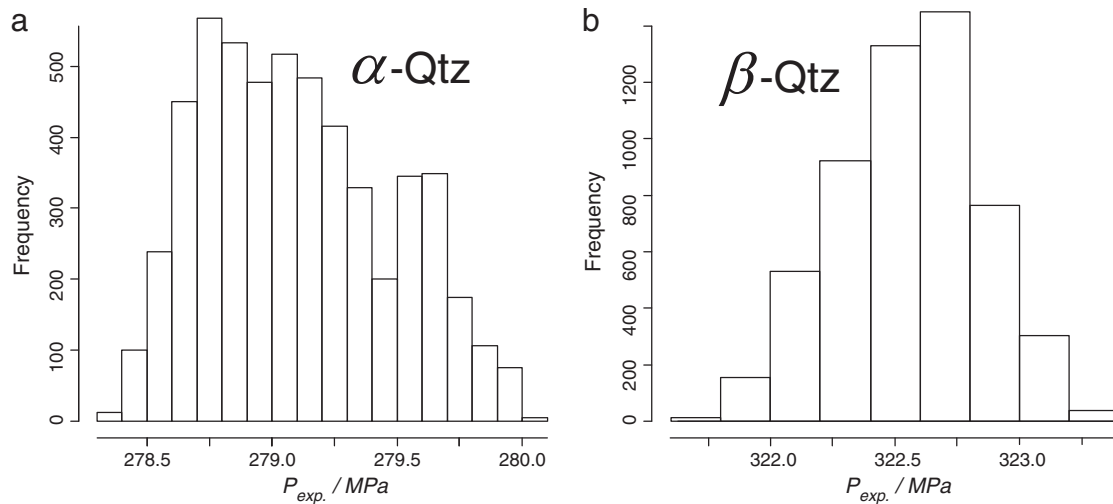


**Fig. 11.** Experimental pressure histograms. (a) The  $\alpha$ -quartz experiment (*GMR009b*) gives the range of  $P_{exp.}$  from 278.3 to 280.1 MPa with the mean value of 279.2 MPa (dashed line). (b) The histogram based on the data of the  $\beta$ -quartz experiment *GMR010b* gives the  $P_{exp.}$  range from 321.7 to 323.3 MPa with a mean value of 322.5 MPa (dashed line). The  $\beta$ -quartz experiments show a normal distribution of the experimental pressure values. Detailed experimental condition properties are summarized in Table 1 and in Appendix A.

Experiment *GMRO10b* in the  $\beta$ -quartz stability field records a variation in molar volumes between 27.45 and 27.52  $\text{cm}^3 \cdot \text{mol}^{-1}$  (Fig. 2b), similar to the previously mentioned experiment in the  $\alpha$ -quartz stability field. Although molar volumes are similar, the expected  $T_h$  are about 3 °C lower than in experiments *GMRO09b*, due to a larger correction of isochores that originate in the  $\beta$ -quartz stability field. The observed  $T_h$  values are in fact slightly lower, but still exceed those values expected from full correction calculations. Again, the application of compressibility and expansion of quartz according to the model of Hosieni et al. (1985) result in overestimated densities. The complementary re-equilibration experiment *RO10b* was performed at approximately 2 MPa lower pressures, corresponding to a variation in molar volumes of 27.56 to 27.63  $\text{cm}^3 \cdot \text{mol}^{-1}$  (Fig. 2b). Homogenization temperatures should theoretically increase by +0.9 to +1.6 °C reflecting these slightly different experimental conditions. However, the observed changes in  $T_h$  range up to +2.5 °C, which must correspond to an additional process caused by leakage of the fluid inclusions. This process is considered to be the  $\alpha$ - $\beta$  transition of quartz that induced a series of micro-cracks or enhanced local diffusion of  $\text{H}_2\text{O}$ , resulting in a lower density. The relative change in density is only about -0.6% at a hydrothermal pressure of 320 MPa.

#### 5.4. Compositional and density changes in re-equilibration experiments with $\text{D}_2\text{O}$

Re-equilibration experiments with  $\text{D}_2\text{O}$  (*R009a*, *R010a*, and *R013a*) at the same temperature and pressure, result in efficient diffusion processes of  $\text{H}_2\text{O}$  out of the inclusions and  $\text{D}_2\text{O}$  into the inclusions. These results are consistent with the experiments of Doppler et al. (2013). The mobility of both components is clearly illustrated by changes in ice melting temperature of individual inclusions (Table 2, Fig. 9). Mixing of  $\text{H}_2\text{O}$  and  $\text{D}_2\text{O}$  at constant experimental conditions also results in changes in homogenization temperatures. The combined changes of  $T_m(\text{ice})$  and  $T_h$  with increasing fraction of  $\text{D}_2\text{O}$  is illustrated in Fig. 9.

The synthetic fluid inclusion assemblage from the re-equilibration experiment in the  $\alpha$ -quartz stability field (*R009a*) display changes in both  $T_m(\text{ice})$  and  $T_h$  consistent with the theoretical predictions (Fig. 9a). Therefore, the exchange of  $\text{H}_2\text{O}$  and  $\text{D}_2\text{O}$  according to the induced fugacity gradients is the only process responsible for changes in the fluid inclusions and the variation in change depends on the size and the position of inclusions in the host relative to the re-equilibrating fluid.

The re-equilibration experiment in the  $\beta$ -quartz stability field (*R010a*) with the same molar volume as in the  $\alpha$ -quartz stability field results in larger shifts in  $T_m(\text{ice})$  and  $T_h$  (Fig. 9b). The maximum  $T_m(\text{ice})$  is +3.7 °C which indicates a nearly total exchange of  $\text{H}_2\text{O}$  and  $\text{D}_2\text{O}$  in the relative short experimental run time of 19 days. However, the expected shift in  $T_h$  due to this process is much higher than the observed  $T_h$  in the sample (Fig. 9b). In other words, the observed homogenization temperature is higher than expected from  $\text{H}_2\text{O}$  and  $\text{D}_2\text{O}$  diffusion alone. The relative change in density in experiment *R010a* according to these considerations is about -1.5%. Again, the  $\alpha$ - $\beta$  transition of quartz must have induced a total volume increase postulated again to be via the formation of micro-cracks around individual inclusions, resulting in a lower density.

The theoretically predicted changes in  $T_m(\text{ice})$  and  $T_h$  is larger in re-equilibration experiment *R013a* (Fig. 9b) in the  $\beta$ -quartz stability field at the same temperature compared to the experiment *R010a* at lower pressures (280 MPa). The observed changes in temperature are similar to those measured in *R010a*. Consequently, the change in  $T_h$  is much more dramatic after the diffusion process that exchanges  $\text{H}_2\text{O}$  and  $\text{D}_2\text{O}$ . Therefore, the density loss due to the  $\alpha$ - $\beta$  transition of quartz is more efficient at lower pressures, and reaches relative values up to -3.0% in experiment *R013a*. The increase of loss towards lower pressures is consistent with observations at room pressures, where decrepitation of fluid inclusions at the  $\alpha$ - $\beta$  transition causes a total loss of the fluid content in inclusions (e.g. Hall and Bodnar, 1989).

#### 5.5. Comparison with previous re-equilibration experiments that are affected by the $\alpha$ - $\beta$ quartz transition

Four phenomena have been identified by a number of fluid inclusion researchers that can affect fluid inclusions composition and density in quartz at high temperature. These are: 1) fugacity gradient; 2) pressure gradient; 3)  $\alpha$ - $\beta$  quartz transition; and 4) microstructure. All of these factors promote diffusion of fluid components (mainly  $\text{H}_2\text{O}$ ) through the crystal lattice and promote decrepitation, leakage, or incomplete decrepitation. Our study illustrates the effect of only the  $\alpha$ - $\beta$  quartz transition on the diffusion of  $\text{H}_2\text{O}$  and  $\text{D}_2\text{O}$  as a water tracer. Although fluid inclusion changes are clearly enhanced if the  $\alpha$ - $\beta$  quartz transition is crossed, mainly at relative lower pressures, while these changes become less pronounced at increasing pressures. Most of the re-equilibration experiments published by Sterner and Bodnar (1989) were performed in the  $\beta$ -quartz stability field. Pure  $\text{H}_2\text{O}$  synthetic fluid inclusions were subjected to high internal overpressures (up to 400 MPa) simultaneously with high gradients in  $\text{H}_2\text{O}$  fugacity. Moreover, the  $\alpha$ - $\beta$  quartz transition was crossed in most experiments. The results were mainly analyzed in terms of general changes in homogenization temperatures of a fluid inclusion assemblage, without knowledge of changes in individual inclusions. Internal overpressure and the  $\alpha$ - $\beta$  quartz transition may result in uncontrolled total volume increase of fluid inclusions (incomplete decrepitation), and over-fugacity results in diffusion of  $\text{H}_2\text{O}$  out of the inclusions. Each of these processes result in the observed decrease in  $\text{H}_2\text{O}$  density in fluid inclusions, but the individual contribution of each process cannot be quantified. At the selected temperatures of the experimentation (700 to 900 °C), diffusion is a highly efficient process for fluid component transfer through the quartz lattice (Doppler et al., 2013). Diffusion of  $\text{H}_2\text{O}$  according to the imposed gradients resulted in a decrease of internal pressure in addition to the loss of  $\text{H}_2\text{O}$ , calculated with the software "ReqDiF" (Bakker, 2009). At equilibrium condition, i.e. when the internal and external fugacities of  $\text{H}_2\text{O}$  are equal, the initial internal overpressure is converted into an internal under-pressure, unlike the considerations of Sterner and Bodnar (1989). In addition the experiments with internal under-pressures (Sterner and Bodnar, 1989) are submitted to similar processes. However, diffusion of  $\text{H}_2\text{O}$  into the inclusions according to fugacity gradients is not able to produce an internal overpressure (see Bakker, 2009).

Re-equilibration experiments with synthetic fluid inclusions (10 mass% NaCl) from Vityk and Bodnar (1995) that simulate "nearly isothermal decompression" or "nearly isothermal compression" were performed at the exact temperature-pressure conditions of the  $\alpha$ - $\beta$  quartz transition. The set-up of the Vityk and Bodnar (1995) experiments did not allow any direct comparison of specific fluid inclusions before and after re-equilibration, because individual inclusions were not characterized prior to re-equilibration. The stepwise temperature and pressure changes result in inclusions entrapment at multiple conditions, during the variable re-equilibration conditions. The results were mainly given in terms of texture (morphology of fluid inclusion assemblages) and expected general changes in homogenization temperatures of a fluid inclusion assemblage, according to the empirical equations of Bodnar and Vityk (1994). These experiments were subjected to huge gradients in  $\text{H}_2\text{O}$  fugacity, which must have resulted in diffusion at these conditions. NaCl is assumed to remain immobile, consequently, a change in salinity must have occurred, but was not reported. Similar to the experiments of Sterner and Bodnar (1989),  $\text{H}_2\text{O}$  fugacity gradients, pressure gradients and the  $\alpha$ - $\beta$  quartz transition may have affected the properties of the synthetic inclusions, but the individual contribution to the change in homogenization temperatures (molar volume) of each of these phenomenon is unknown.

#### 5.6. Implications for the interpretation of natural fluid inclusions

The  $\alpha$ - $\beta$  quartz transition may occur in metamorphic rocks that are formed at amphibolite and granulite facies, in addition to contact

metamorphism. Fluid inclusions that are trapped under these conditions in quartz may be subjected to density loss due to  $\alpha$ - $\beta$  quartz transition during exhumation of the rock. Our experimental work has illustrated that the density loss is only about  $-0.5\%$  at 320 MPa hydrostatic pressure, and rapidly increases towards lower pressures. Consequently, the  $\alpha$ - $\beta$  quartz transition does not affect fluid densities at higher pressure, at metamorphic conditions that occur in subduction zones and continental orogenic belts. However, the retrograde segment of a specific P–T–t path (pressure–temperature–time) for a rock may follow a decreasing temperature during uplift and erosion, which may reach conditions below 300 MPa around 600 °C. Fluid inclusions in quartz in these rocks are most certainly affected by density-loss due to the  $\alpha$ - $\beta$  quartz transition.

## 6. Conclusions

Potential effects of the  $\alpha$ - $\beta$  quartz phase transition on the properties of fluid inclusions were investigated by re-equilibration experiments with synthesized H<sub>2</sub>O-rich inclusions. Fluid inclusions were synthesized in the  $\alpha$ -quartz and  $\beta$ -quartz stability fields with equal molar volumes, close to the phase transition. Complementary re-equilibration experiments were performed at the same experimental pressure and temperature to avoid pressure gradients, fugacity gradients and deformation. Therefore, any changes in fluid properties of the inclusions were caused only by the  $\alpha$ - $\beta$  quartz transition.

Shape changes are independent of the used fluid composition, either H<sub>2</sub>O or D<sub>2</sub>O. The majority of the originally regular and equant fluid inclusions reveal only minor changes in shape after re-equilibration. Only elongated and irregular fluid inclusions are affected by shape changes, and reach relative values of 55% and 60% in shape parameters in the  $\alpha$ -quartz and  $\beta$ -quartz re-equilibration experiments, respectively. Re-equilibration experiments with pure H<sub>2</sub>O demonstrate only minor changes in fluid inclusion properties in the  $\alpha$ -quartz stability field. These experiments also reveal the sensitivity of changes in fluid inclusion density due to minor changes in experimental conditions. Fluid inclusions properties are significantly changed to lower densities after the re-equilibration experiment in the  $\beta$ -quartz, due to the  $\alpha$ - $\beta$  quartz phase transition. The magnitude of the hydrothermal pressure affects the amount of density loss. At 320 MPa, a density loss of approximately  $-0.6\%$  is observed, whereas density loss up to  $3.0\%$  is measured at 280 MPa after 19 days of experimentation.

Additional fugacity gradients were induced with pure D<sub>2</sub>O re-equilibration experiments. The mobility of both H<sub>2</sub>O and D<sub>2</sub>O at the same conditions illustrates the efficiency of diffusion processes within 19 days. Fluid inclusions contain up to 53 mol% D<sub>2</sub>O after the re-equilibration experiment in the  $\alpha$ -quartz stability field, but up to 97 mol% D<sub>2</sub>O after re-equilibration in the  $\beta$ -quartz stability field. The observed changes in homogenization temperatures illustrate that density-loss due to the  $\alpha$ - $\beta$  quartz phase transition is an additional process that affects inclusions from the  $\beta$ -quartz re-equilibration experiments, and that the density-loss caused by the  $\alpha$ - $\beta$  quartz phase transition is more efficient at lower pressures.

Supplementary data to this article can be found online at <http://dx.doi.org/10.1016/j.lithos.2014.03.018>.

## Acknowledgments

We would like to thank the Austrian Science Fund (FWF) for financial support (project no. P 22446-N21). Alfons van den Kerkhof and an anonymous reviewer are thanked for their fruitful critics and suggestions. Comments from M. Scambelluri (editor) clearly improved the manuscript.

## References

- Audétat, A., Günther, D., 1999. Mobility and H<sub>2</sub>O loss from fluid inclusions in natural quartz crystals. *Contributions to Mineralogy and Petrology* 137, 1–14.
- Ayllón, F., Bakker, R.J., Warr, L.N., 2003. Re-equilibration of fluid inclusions in diagenetic-anchizone rocks of the Ciñera-Matallana coal basin (NW Spain). *Geofluids* 3, 49–68.
- Bakker, R.J., 2003. Package FLUIDS 1. Computer programs for analysis of fluid inclusion data and for modelling bulk fluid properties. *Chemical Geology* 194, 3–23.
- Bakker, R.J., 2009. Package FLUIDS. Part 3. Correlations between equations of state, thermodynamics and fluid inclusions. *Geofluids* 9 (1), 63–74.
- Bakker, R.J., Diamond, L.W., 1999. Re-equilibration of synthetic CO<sub>2</sub>–H<sub>2</sub>O fluid inclusions in quartz: isofugacity experiments. *Terra Nostra* v. 9/96, 20–21.
- Bakker, R.J., Diamond, L.W., 2006. Estimation of volume fractions of liquid and vapor phases in fluid inclusions, and definition of inclusion shapes. *American Mineralogist* 91, 635–657.
- Bakker, R.J., Jansen, J.B.H., 1990. Preferential water leakage from fluid inclusions by means of mobile dislocations. *Nature* 345, 58–60.
- Bakker, R.J., Jansen, J.B.H., 1991. Experimental post-entrapment water loss from synthetic CO<sub>2</sub>–H<sub>2</sub>O inclusions in natural quartz. *Geochimica et Cosmochimica Acta* 55, 2215–2230.
- Bakker, R.J., Jansen, J.B.H., 1993. Calculated fluid evolution path versus fluid inclusion data in the COHN system as exemplified by metamorphic rocks Rogaland SW Norway. *Journal of Metamorphic Geology* 11, 426–440.
- Bakker, R.J., Jansen, J.B.H., 1994a. A mechanism for preferential H<sub>2</sub>O leakage from fluid inclusions in quartz, based on TEM observations. *Contributions to Mineralogy and Petrology* 116, 7–20.
- Bakker, R.J., Jansen, J.B.H., 1994b. Raman Spectra of fluid and crystal mixtures in the systems H<sub>2</sub>O, H<sub>2</sub>O–NaCl and H<sub>2</sub>O–MgCl<sub>2</sub> at low temperatures: applications to fluid-inclusion research. *The Canadian Mineralogist* 42, 1283–1314.
- Bodnar, R.J., Sterner, S.M., 1987. Synthetic fluid inclusions. In: Barnes, H.L., Ulmer, G.C. (Eds.), *Hydrothermal Experimental Techniques*. Wiley, New York, pp. 423–457.
- Bodnar, R.J., Vityk, M.O., 1994. Interpretation of microthermometric data for NaCl–H<sub>2</sub>O fluid inclusions. In: De Vivo, B., Frezzotti, M.L. (Eds.), *Fluid Inclusions in Minerals: Methods and Applications*. Virginia Polytechnic Inst State Univ., Blacksburg, VA, pp. 117–130 (9).
- Branlund, J.M., Hofmeister, A.M., 2007. Thermal diffusivity of quartz to 1,000 °C: effects of impurities and the  $\alpha$ - $\beta$  phase transition. *Physics and Chemistry of Minerals* 34, 581–595.
- Crank, J., 1975. *The Mathematics of Diffusion*. Oxford science publications, Oxford.
- Diamond, L.W., Tarantola, A., Stünitz, H., 2010. Modification of fluid inclusions in quartz by deviatoric stress. II: experimentally induced changes in inclusion volume and composition. *Contributions to Mineralogy and Petrology* 160, 845–864.
- Doppler, G., Bakker, R.J., Baumgartner, M., 2013. Fluid inclusion modification by H<sub>2</sub>O and D<sub>2</sub>O diffusion: the influence of inclusion depth, size, and shape in re-equilibration experiments. *Contributions to Mineralogy and Petrology* 165, 1259–1274.
- Haar, L., Gallagher, J.S., Kell, G.S., 1984. NBS/NRC steam tables. Hemisphere Publishing Corporation, Washington.
- Hall, D., Bodnar, R.J., 1989. Comparison of fluid inclusion decrepitation and acoustic emission profiles of Westerly granite and Sioux quartzite. *Tectonophysics* 168, 283–296.
- Heuer, A.H., Nord Jr., G.L., 1976. Polymorphic phase transitions in minerals. *Electron Microscopy in Mineralogy* 274–303.
- Hill, P.G., MacMillan, C.R.D., Lee, V., 1982. A fundamental equation of state for heavy water. *Journal of Physical and Chemical Reference Data* 11 (1), 1–14.
- Hladky, G., Wilkins, R.W.T., 1987. An evaluation of fluid inclusion decrepitation using quartz from the Kingsgate molybdenite–bismuth deposits, New South Wales, Australia. *12. N. Jb. Miner. Mh., Stuttgart* pp. 537–549.
- Hosieni, K.R., Howald, R.A., Scanlon, M.W., 1985. Thermodynamics of the lambda transition and the equation of state of quartz. *American Mineralogist* 70, 782–793.
- Kerrick, D.M., 1987. Cold-seal systems. In: Ulmer, G.C., Barnes, H.L. (Eds.), *Hydrothermal Experimental Techniques*. Wiley, New York, pp. 293–323.
- Laughner, J.W., Cline, T.W., Newnham, R.E., Cross, L.E., 1979. Acoustic emissions from stress-induced dauphiné twinning in quartz. *Physics and Chemistry of Minerals* 4 (2), 129–137.
- Roedder, E., 1984. Fluid inclusions. *Mineralogical Society of America, Review in Mineralogy* 12, 644.
- Samson, I., Anderson, A., Marshall, D., 2003. *Fluid Inclusions: analysis and Interpretation: Mineralogical Association of Canada. Short Course*, vol. 32 p. 370.
- Schmidt-Mumm, 1991. Low frequency acoustic emission from quartz upon heating from 90 to 610 °C. *Physics and Chemistry of Minerals* 17, 545–553.
- Sterner, Bodnar, 1989. Synthetic fluid inclusions – VII. Re-equilibration of fluid inclusions in quartz during laboratory-simulated metamorphic burial and uplift. *Journal of Metamorphic Geology* 7, 243–260.
- Sterner, S.M., Bodnar, R.J., 1991. Synthetic fluid inclusions. X: experimental determination of P–V–T–X properties in the CO<sub>2</sub>–H<sub>2</sub>O system to 6 kb and 700 °C. *American Journal of Science* 291, 1–54.
- Tarantola, A., Diamond, L.W., Stünitz, H., 2010. Modification of fluid inclusions in quartz by deviatoric stress I: experimentally induced changes in inclusion shapes and microstructures. *Contributions to Mineralogy and Petrology* 160, 825–843.
- Vityk, M.O., Bodnar, R.J., 1995. Textural evolution of synthetic fluid inclusions in quartz during re-equilibration, with applications to tectonic reconstruction. *Contributions to Mineralogy and Petrology* 121, 309–323.
- Vityk, M.O., Bodnar, R.J., 1998. Statistical microthermometry of synthetic fluid inclusions in quartz during decompression re-equilibration. *Contributions to Mineralogy and Petrology* 132, 149–162.